JOURNAL OF BIOMOLECULAR STRUCTURE AND DYNAMICS
https://doi.org/10.1080/07391102.2020.1850358

In vitro antimicrobial, physicochemical, pharmacokinetics and molecular docking studies of benzoyl uridine esters against SARS-CoV-2 main protease

Mohammed Mahbubul Matin[a], Monir Uzzaman[a,b], Shagir Ahammad Chowdhury[a] and Md. Mosharef Hossain Bhuiyan[a]

[a]Bioorganic and Medicinal Chemistry Laboratory, Department of Chemistry, Faculty of Science, University of Chittagong, Chattogram, Bangladesh; [b]Faculty of Engineering, Department of Applied Chemistry and Biochemical Engineering, Shizuoka University, Hamamatsu, Japan

Communicated by Ramaswamy H. Sarma

ABSTRACT

Different esters were found potential against microorganisms, and could be a better choice to solve the multidrug resistant (MDR) pathogenic global issue due to their improved biological and pharmacokinetic properties. In this view, several 4-*t*-butylbenzoyl uridine esters **4–15** with different aliphatic and aromatic groups were synthesized for antimicrobial, physicochemical and biological studies. *In vitro* antimicrobial tests against nine bacteria and three fungi along with prediction of activity spectra for substances (PASS) indicated promising antifungal functionality of these uridine esters compared to the antibacterial activities. In support of this observation their cytotoxicity and molecular docking studies have been performed against lanosterol 14α-demethylase (CYP51A1) and *Aspergillus flavus* (1R51). Significant binding affinities were observed against SARS-CoV-2 main protease (7BQY) considering hydroxychloroquine (HCQ) as standard. ADMET predictions were investigated to evaluate their absorption, metabolism and toxic properties. Most of the uridine esters showed better results than that of the HCQ. Overall, the present study might be useful for the development of uridine-based novel MDR antimicrobial and COVID-19 drugs.

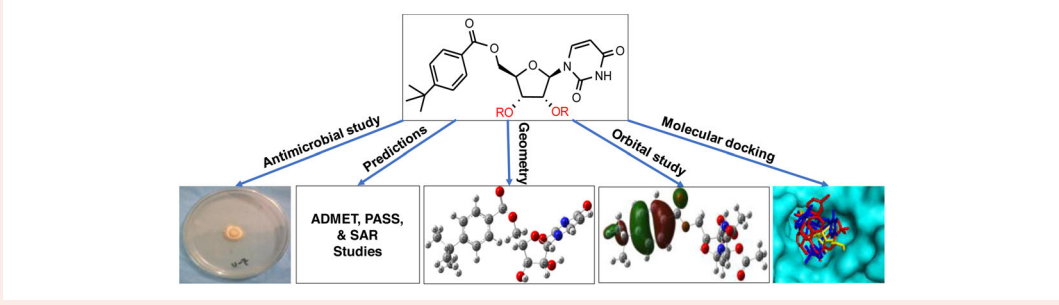

ARTICLE HISTORY
Received 20 August 2020
Accepted 6 November 2020

KEYWORDS
Uridine esters; density functional theory; thermodynamic and orbital properties; antimicrobial activities; PASS and ADMET predications; SARS-CoV-2 main protease

1. Introduction

Uridine (**1**), a natural and necessary nucleoside, is one of the four basic components of ribonucleic acid (RNA). It is a structural element of many bioactive compounds, and it has crucial role in the pyrimidine metabolism of the brain. Uridine and its nucleotide derivatives may also have an additional role in the function of the central nervous system as signaling molecules (Dobolyi et al., 2011). It has anti depression activity, asthmatic airway inflammation, hepatocyte proliferation (Carlezon et al., 2005). Uridine has sleep-promoting and anti-epileptic effects, might affect mood, improves memory function and influences neuronal plasticity (Siegel et al., 2017). Uridine, sometimes, has been recognized as playing a role in preserving and enhancing hepatic mitochondrial function in the face of challenge by certain liver toxins (Banasch et al., 2006). In addition, uridine (**1**) and some of its biological derivatives behave as antimetabolites, when their extracellular concentrations are higher than those physiological levels (Strasser et al., 2006; Yamamoto et al., 2011).

Many advantageous findings were reported for the uridine derivatives especially its esters. For example, uridine 5′ esters showed neuroprotective effect and is capable of compensating the harmful effect of neurotoxins with the increase the 5-HT and 5-HIAA levels (Susilo, 2008). 3′,4′-Uridine acetonide (**2**, Figure 1) showed a differential effect and a higher activity over cell viability on MCF-7 human cancer breast cell line than for the CHO-K1 cell line (Escober et al., 2016). Some uridine esters were found to exhibit promising antimicrobial

CONTACT Mohammed Mahbubul Matin mahbubchem@cu.ac.bd Bioorganic and Medicinal Chemistry Laboratory, Department of Chemistry, Faculty of Science, University of Chittagong, Chattogram 4331, Bangladesh

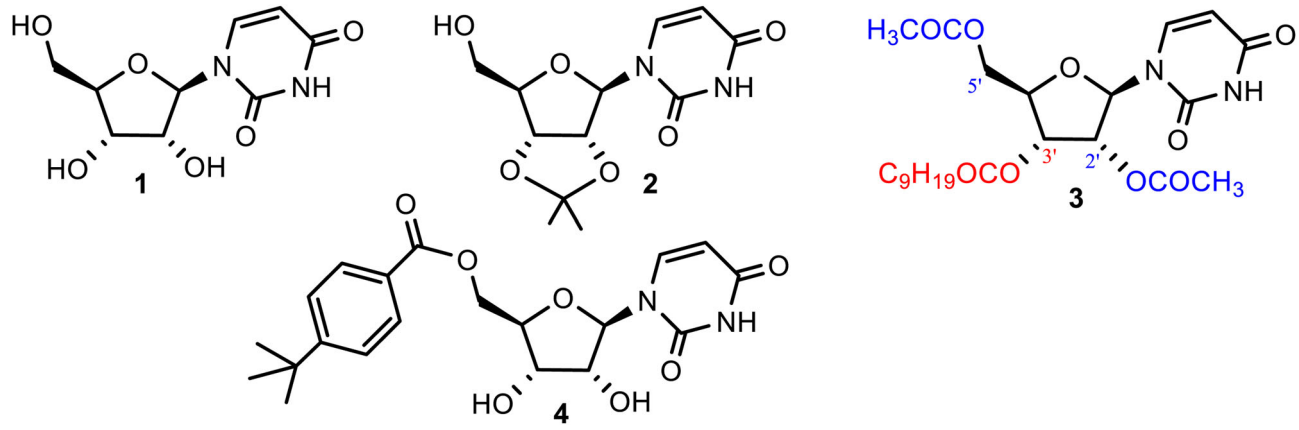

Figure 1. Structures of **1**–**4**.

properties (Kabir, Matin, & Kawsar, 1998; Kabir, Matin, Kawsar, & Anwar, 1998; Kabir, Matin, Mridha, et al., 1998; Kabir et al., 1998a, 1998b) such as 3′-*O*-decanoyl-2′,5′-di-*O*-acetyluridine (**3**) was found very active against *E. coli* (Kabir et al., 2002). Thus, it has been proven that the uridine derivatives especially acyl esters can be used as drugs in order to treat, for instance, Parkinson, Alzheimer, Chorea Huntington or depression with cellular regulatory functions (Escober et al., 2016).

Although uridine analogues (e.g. doxifluridine) have shown higher activities in the treatment of viral and cancer treatment, their efficiency is sometimes reduced by the appearance of resistance mechanisms (De Clercq, 2011). Hence, search for newer analogues of uridine (nucleoside) got more attention especially esterification of its sugar moiety (Du et al., 2018). However, investigations indicated that selective esterification (acylation) uridine (**1**) creates difficulties due to the presence of one 1° OH group, two 2° OH groups and a NH group. Hence, various methods like direct acylation (Matin, Bhattacharjee, et al., 2019; Matin, Bhuiyan, et al., 2019; Matin, Chakraborty, et al., 2020; Matin, Hasan, et al., 2020; Matin, Roshid, et al., 2020), dibutyltin oxide (DBTO) method (Kabir, Matin, & Kawsar, 1998; Kabir, Matin, Kawsar, & Anwar, 1998; Kabir, Matin, Mridha, et al., 1998; Kabir et al., 1997, 1998a, 1998b), coupling technique (Steglich esterification) (Clayden et al., 2012), protection–deprotection (Matin et al., 2017) and enzymatic method (Du et al., 2018) were reported. Among these methods, direct method generally furnished 5′-*O*-substituted esters (Kabir, Matin, & Kawsar, 1998; Kabir, Matin, Kawsar, & Anwar, 1998; Kabir, Matin, Mridha, et al., 1998; Kabir et al., 1997, 1998a, 1998b) whereas DBTOmethod gave 3′-*O*-substituted products (Kabir, Matin, & Kawsar, 1998; Kabir, Matin, Kawsar, & Anwar, 1998; Kabir, Matin, Mridha, et al., 1998; Kabir et al., 1997, 1998a, 1998b, 2002). However, in most of the cases direct method gave higher yield(s) with lower cost (Matin, 2014; Matin et al., 2017). Chowdhury et al. (2016) applied direct method with hindered 4-*t*-butylbenzoyl chloride in pyridine at −5 °C and afforded the 5′-*O*-(4-*t*-butylbenzoyl)uridine (**4**) in excellent yield.

Now-a-days, emergence of multiple drug resistant (MDR) pathogenic organisms, and corona virus disease 2019 (COVID-19) are global concern (Ghosh et al., 2020; Lakshmi et al., 2020; Wahedi et al., 2020) in addition to numerous obstacles encountered on delivery to the site of microbial infection. Many researchers are engaged to overcome these situations (Awual, 2017; Laws et al., 2020; Matin, 2008; Sharavanan et al., 2020). However, there is urgent need for establishment of new chemotherapeutic agents with novel mode of action to combat with these MDR organisms, and SARS CoV-2 (severe acute respiratory syndrome corona virus-2). In this regard as well as our continuous effort to find novel drugs (Matin, 2014; Matin & Ibrahim, 2010; Matin et al., 2015) we report herein the *in vitro* antimicrobial efficacy of several uridine-based esters **4**–**15** with different aliphatic and aromatic chains against eleven pathogens, molecular docking against lanosterol 14α-demethylase (3LD6), *A. flavus* (1R51) and corona virus (SARS CoV-2) main protease (Mpro; 7BQY) along with prediction of activity spectra for substances (PASS). Also, attempts have been taken to optimize some acylated uridine derivatives to investigate their physicochemical behavior on the basis of DFT approach with cytotoxicity, and ADMET properties.

2. Material and methods

2.1. Materials: uridine esters 4–15

In our present study, twelve uridine-based esters with different side chain length and different groups **4**–**15** were used as test chemicals. These compounds (mainly 5′-*O*-*t*-butylbenzoyl esters of uridine), as presented in Figure 2, were synthesized from **1** by direct method and well characterized earlier (Chowdhury et al., 2016). For comparative study, uridine (**1**), standard antibacterial antibiotic ampicillin and antifungal antibiotic nystatin were also used.

2.2. Pass predication

Web-based PASS (http://www.pharmaexpert.ru/ PASSonline/index.php) was used for the prediction of biological spectrum of these uridine derivatives (Matin et al., 2016). Initially, structures of the uridine esters were drawn, and then, converted into their SD file formats which were used to predict biological spectrum using PASS online software. This program is designed to anticipate a plethora of biological activities with 90% accuracy. PASS results are designated as Pa

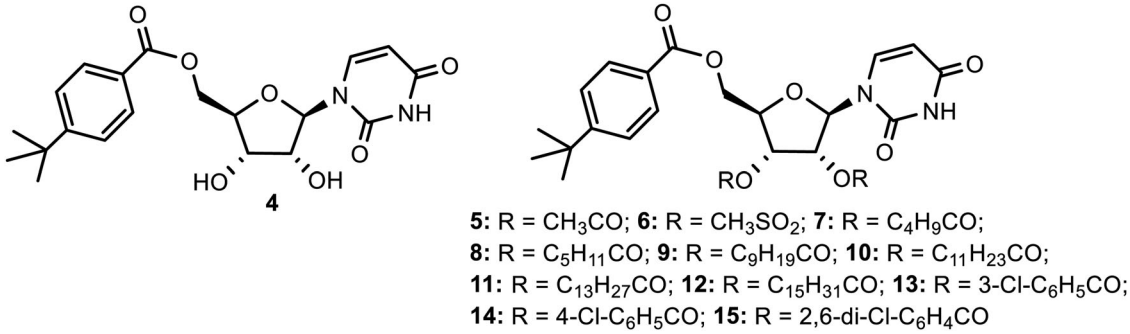

Figure 2. Structures of **4**–**15**.

Table 1. Name of the pathogenic microorganisms.

Sl.	Strain	Reference	Source
Gram-positive bacteria			
(i)	*Bacillus cereus*	BTCC 19	Gastrointestinal tract
(ii)	*Bacillus megaterium*	BTCC 18	Clinical strains
(iii)	*Bacillus subtilis*	BTCC 17	Gastrointestinal tract
(iv)	*Staphylococcus aureus*	ATCC 6538	Dairy cows
Gram-negative bacteria			
(v)	*Escherichia coli*	ATCC 25922	Clinical isolate
(vi)	*Shigella dysenteriae*	AE 14369	Milk & dairy products
(vii)	*Salmonella paratyphi*	ATCC 11511	Clinical isolate
(viii)	*Salmonella typhi*	AE 14612	Raw meat
(ix)	*Vibrio cholera*	ICDDR, B	Stool sample
Name of the fungi			Type of organism
(i)	*Aspergillus acheraccus*		Human pathogenic
(ii)	*Aspergillus flavus*		Human pathogenic
(iii)	*Macrophomina phaseolina*		Human pathogenic

(probability for active compound) and Pi (probability for inactive compound). Being probabilities, the Pa and Pi values vary from 0.000 to 1.000 and in general, $Pa + Pi \neq 1$, since these probabilities are calculated independently. Only the activities with $Pa > Pi$ are considered as possible for a particular drug. The PASS prediction results were interpreted and used in a flexible manner, viz. (i) when $Pa > 0.7$, the chance to find the activity experimentally is high, (ii) if $0.5 < Pa < 0.7$, the chance to find the activity experimentally is less, but the compound is probably not so similar to known pharmaceutical agents and (iii) if $Pa < 0.5$, the chance to find the activity experimentally is less, but the chance to find a structurally. So, the predicted activity of spectrum of a drug is known as its intrinsic property.

2.3. *In vitro* antimicrobial activity test

2.3.1. Test organisms

The tested microorganisms (bacteria and fungi) were collected from the Pharmacology laboratory, Department of Physiology, Biochemistry & Pharmacology, Faculty of Veterinary Medicine, Chittagong Veterinary and Animal Science University, Chattogram, Bangladesh. As shown in Table 1, nine human pathogenic bacteria and three plant pathogenic fungi were used for the antimicrobial evaluation.

2.3.2. Screening of antibacterial activity

In vitro antibacterial activities of uridine **4**–**15** were conducted by paper disc diffusion method (Kabir et al., 2003; Matin et al., 2013), which was determined by the presence or absence of diameter of zone of inhibition (in mm). In this method, initially a 2% solution of the uridine compound(s) in DMF was prepared. Mueller-Hinton (agar and broth) medium was used to culture the bacteria. Paper disc of 4 mm in a diameter and petri plate of 70 mm in a diameter was used throughout the experiment. These paper discs were sterilized in an autoclave and dried at 150 °C in an electric oven. Then, the discs were socked with test compound(s) at the rate of 100 μg (dry weight) per disc. These paper discs were put in the petri-plates and were incubated at 37 °C for 48 h for growth of test organisms followed by the cooling for 4 h at low temperature (4 °C). The test chemicals diffused from disc to the surrounding medium by this time. The growth inhibition was calculated at 24 h intervals for two days. Each experiment was carried out three times. All the results were compared with the standard antibacterial antibiotic ampicillin (50 μg/disc, brand name Decapen, Beximco Pharmaceuticals Ltd., Bangladesh). Ampicillin was also used as a positive control and proper control was maintained with DMF without chemicals under identical conditions.

2.3.3. Screening of mycelial growth

The *in vitro* antifungal screening of the synthesized uridine derivatives (**4**–**15**) were investigated employing food poisoning technique (Kabir, Matin, & Kawsar, 1998; Kabir, Matin, Kawsar, & Anwar, 1998; Kabir, Matin, Mridha, et al., 1998; Kabir et al., 1998a, 1998b; Matin, 2014). Sabouraud potato dextrose agar (PDA, agar and broth) medium was used for the culture of fungi. Necessary amount of medium was taken in a conical flask separately and was sterilized in an autoclave (at 121 °C and 15 psi) for 15 min. After autoclaving, weighed amount of test chemical (2% in DMF) was added to the sterilized medium in conical flask at the point of pouring to obtain desired concentration. The flask was shaken thoroughly to mix the chemical with the medium homogeneously before pouring. The medium with definite concentration (2%) of chemical was poured at the rate of 100 μg/mL PDA in sterilized glass petri dishes individually and subjected for incubation. Finally, linear mycelial growth of fungus was measured after 2–5 days (24 h interval) of incubation. The percentage of radial mycelial growth inhibition of the test fungus was calculated using the following equation:

$$I = \left\{\frac{(C-T)}{C}\right\} \times 100$$

Where, I = percentage of inhibition, C = diameter of the fungal colony in control (DMF), T = diameter of the fungal colony in treatment. In all the cases, the results were compared with standard antifungal antibiotic nystatin (100 μg/mL medium, brand name Fungistin, Beximco Pharmaceuticals Ltd., Bangladesh). Proper control was maintained separately and with sterilized PDA medium without chemical and three replications were prepared for each treatment.

2.4. Computational details: DFT

Quantum mechanical (QM) methods has gained attention on calculation of thermodynamic properties, molecular orbital features, dipole moment and as well as interpretation of different types of interactions. Molecular geometry optimization and further modification of all uridine derivatives carried out using Gaussian 16 program. All the structures were optimized using density functional theory (DFT) employing Becke's (B) three-parameter hybrid model, Lee, Yang and Parr's (LYP) correlation functional under 3-21G basis set (Kruse et al., 2012). Initial optimization of all compounds was performed in the gas phase. Dipole moment, electronic energy, enthalpy and free energy are calculated for all the compounds.

Frontier molecular orbital features HOMO (highest occupied molecular orbital), LUMO (lowest unoccupied molecular orbital) were calculated at the same level of theory. For each of the structure HOMO-LUMO gap($\Delta\varepsilon$), hardness (η), softness (S) and chemical potential (μ) were calculated from the energies of frontier HOMO and LUMO as reported considering Parr and Pearson interpretation of DFT and Koopmans theorem (Pearson, 1986) on the correlation of ionization potential and electron affinities with HOMO and LUMO energy (ε). Hardness (η), softness (S) and chemical potential (μ) are calculated by using the following equations:

$$\begin{aligned} \text{Gap } (\Delta\varepsilon) &= (\varepsilon\text{LUMO} - \varepsilon\text{HOMO});\ \eta \\ &= (\varepsilon\text{LUMO} - \varepsilon\text{HOMO})/2;\ \text{S} = 1/\eta;\ \mu \\ &= (\varepsilon\text{LUMO} + \varepsilon\text{HOMO})/2 \end{aligned}$$

2.4.1. Protein preparation and visualization

The 3D crystal structure of main protease of COVID-19 (7BQY), lanosterol 14α-demethylase (3LD6/CYP51A1) and *A. flavus* (1R51) was obtained in pdb format from online protein data bank (PDB) database (Lucido et al., 2016). All hetero atoms, inhibitors and water molecules were erased using PyMol (version 1.3) software packages. Energy minimization of the protein implemented by Swiss-Pdb viewer software (version 4.1.0) (Matin, Chakraborty, et al., 2020; Matin, Hasan, et al., 2020; Matin, Roshid, et al., 2020). The optimized structures were subjected for molecular docking study against 7BQY, CYP51A1 and 1R51 considering the protein as macromolecule and uridine esters as ligand. Finally, rigid docking simulation was performed by PyRx software (version 0.8) targeting the active site with the center grid box size 48.8375, 65.6838, 59.1841 Å for 7BQY; 61.8544, 61.1656, 70.6697 Å for 3LD6; and 58.4699, 69.9558, 58.3507 Å for 15R1 along *x*, *y* and *z* directions, respectively. After docking, Accelrys Discovery Studio (version 4.1) software was utilized to analyze and visualize the docking results (Wahedi et al., 2020). Docking results are basically calculated as binding affinities of ligand-protease and reported in kcal/mol unit.

2.5. Toxic activity test

For the determination of toxicity of the uridine derivatives we employed brine shrimp lethality assay technique as described by McLaughlin (1991). The tested compounds were dissolved in DMSO, and prepared 20, 40, 80 and 160 μL by adding NaCl solution to each vial up to 1 mL volume which were designated as type- A, B, C and D, respectively. Three sets of experiment were done for each concentration and 10 brine shrimps nauplii were placed in each vial. A control experiment was performed in a vial containing 10 nauplii in 1 mL seawater. After 24 h and 48 h of incubation at room temperature, the vials were observed using a magnifying glass and the number of survivors in each vial was counted and noted. From the data, the average percentage of mortality of nauplii was calculated for each concentration. No deaths were found for controls.

2.6. ADMET calculation

Online computational approaches were made to predict absorption, distribution, metabolism, excretion and toxicity (ADMET) for 5′-*O*-(4-*t*-butylbenzoyl)uridine (**4**) and its 2′,3′-di-*O*-acyl derivatives **5**–**15** (Matin, Chakraborty, et al., 2020; Matin, Hasan, et al., 2020; Matin, Roshid, et al., 2020). The computational prediction of drug could avoid the tremendous cost and time associated with the *in vivo* experiments, and has attracted more and more attention. In the present study, we utilized *in silico* screening approaches employing pkCSM server (http://biosig.unimelb.edu.au). The pkCSM signatures were successfully used across five main different pharmacokinetic property classes to develop predictive regression and classification models (Pires et al., 2015). Firstly, all the structures of uridine esters were drawn in ChemDraw 16.0 to collect InChI Key, isomeric SMILES (simplified molecular-input line-entry system), and SD file format. ADMET of all the uridine esters were predicted by using pkCSM-pharmacokinetics and SwissADME free web tools (http://www.swissadme.ch).

3. Results and discussion

In the present study, twelve uridine esters with different aliphatic and aromatic chains (**4–15**) were selected as test compounds, and screened for their *in vitro* antibacterial and antifungal activities against nine bacteria and, and three phytopathogenic fungi, respectively. Initially, we predicted these

activities using PASS program followed by *in vitro* determination. The observed activities were then rationalized by calculating their physicochemical (DFT method), cytotoxicity (shrimp), molecular docking and ADMET properties. Finally, all these findings were used to summarize their structure–activity relationship (SAR).

Table 2. Predicted biological activity of the uridine-based esters **4**–**15** using PASS software.

	Biological activity							
	Antibacterial		Antifungal		Anti-carcinogenic		Antioxidant	
Drug	Pa	Pi	Pa	Pi	Pa	Pi	Pa	Pi
1	0.397	0.031	0.421	0.046	0.785	0.006	–	–
4	0.320	0.053	0.437	0.042	0.667	0.010	0.168	0.081
5	0.348	0.044	0.486	0.033	0.668	0.010	0.156	0.095
6	0.180	0.137	–	–	0.407	0.030	–	–
7	0.327	0.050	0.526	0.027	0.621	0.012	0.158	0.093
8	0.327	0.050	0.526	0.027	0.621	0.012	0.158	0.093
9	0.327	0.050	0.526	0.027	0.621	0.012	0.158	0.093
10	0.327	0.050	0.526	0.027	0.621	0.012	0.158	0.093
11	0.327	0.050	0.526	0.027	0.621	0.012	0.158	0.093
12	0.327	0.050	0.526	0.027	0.621	0.012	0.158	0.093
13	0.193	0.125	0.436	0.042	0.482	0.021	–	–
14	0.213	0.106	0.441	0.041	0.515	0.018	0.132	0.124
15	0.163	0.152	0.389	0.052	0.467	0.022	0.431	0.10
APC	0.750	0.003	–	–	–	–	–	–
NYS	0.967	0.00	0.986	0.00	0.416	0.028	0.145	0.108

Pa: probability 'to be active'; Pi: probability 'to be inactive'; APC: ampicillin; NYS: nystatin.

Table 3. Inhibition against Gram-positive pathogens by uridine esters.

	Diameter of zone of inhibition in mm (100 μg dw / disc)			
Drug	*B. cereus*	*B. megaterium*	*B. subtilis*	*S. aureus*
1	13.6 ± 0.39	8.5 ± 0.50	7.5 ± 0.50	NI
4	NI	6.1 ± 0.28	10.3 ± 0.58	9.0 ± 0.34
5	NI	7.4 ± 0.44	NI	NI
6	NI	6.6 ± 0.33	NI	NI
7	NI	NI	NI	NI
8	NI	10.3 ± 0.38	NI	NI
9	NI	9.1 ± 0.50	NI	8.5 ± 0.58
10	NI	12.0 ± 0.33	NI	NI
11	NI	7.0 ± 0.33	NI	NI
12	NI	NI	NI	NI
13	NI	NI	7.0 ± 0.66	NI
14	NI	6.6 ± 0.33	NI	6.5 ± 0.45
15	NI	NI	NI	NI
****AMP**	*18.0 ± 0.51	*16.1 ± 0.64	*19.0 ± 0.58	*22.2 ± 0.24

Data are presented as (Mean ± *SD*).
*Significantly inhibition values.
**Reference antibiotic ampicillin (AMP; 50 μg/disc).
dw: dry weight; NI: no inhibition; NI was observed for control DMF; Values are represented for the triplicate of all the experiments.

3.1. Computational-based biological activities: PASS

Having all the uridine esters **4**–**15**, we predicted their biological spectrum using online PASS software (http://www.pharmaexpert.ru/ PASSonline/index.php). The PASS results in its designated as Pa and Pi form is presented in Table 2.

It was evident from predication Table 2 for uridine esters **4**–**15** showed $0.16 < Pa < 0.35$ for antibacterial and $0.38 < Pa < 0.53$ for antifungal. This clearly indicated that these compounds were more prone against fungi as compared to that of bacterial pathogens. Also, incorporation of mesyl groups, as in compound **6**, totally abolished antifungal potentiality of uridine. Addition of aliphatic acyl chains (C2 to C16, compound **5**, **7**–**12**) increased antifungal activity ($Pa = 0.526$) of uridine (**1**, $Pa = 0.421$), whereas attachment of chloro-substituted benzoyl groups did not enhance reasonably (**13**–**15**, $Pa = 0.389$–0.436). We have also calculated anti-carcinogenic and antioxidant property of these compounds. Thus, PASS predication showed $0.46 < Pa < 0.67$ for anti-carcinogenic and $0.13 < Pa < 0.43$ for antioxidant, which indicated that the uridine esters were more potent as anti-carcinogenic agents than that of antioxidant properties. Interestingly, the results as shown in Table 2, antifungal and anti-carcinogenic properties of uridine esters with saturated aliphatic chains (**5**, **7**–**12**) were found more promising than the sulphonyl ester (**6**) or chloro-substituted benzoyl derivatives (**13**–**15**). These results are in agreement with our previous study for monosaccharide esters (Matin, Chakraborty, et al., 2020; Matin, Hasan, et al., 2020; Matin, Roshid, et al., 2020).

3.2. *In vitro* antimicrobial activities

3.2.1. Antibacterial potentiality of 4–15

For the *in vitro* antibacterial efficacy test we followed disc diffusion method (Kabir et al., 2003). The results of diameter of inhibition zone (mm) of the uridine-based esters **4**–**15** against four Gram-positive, and five Gram-negative bacteria are presented in Table 3 (Figure 3) and Table 4 (Figure 4). It was evident that these esters are less susceptible towards

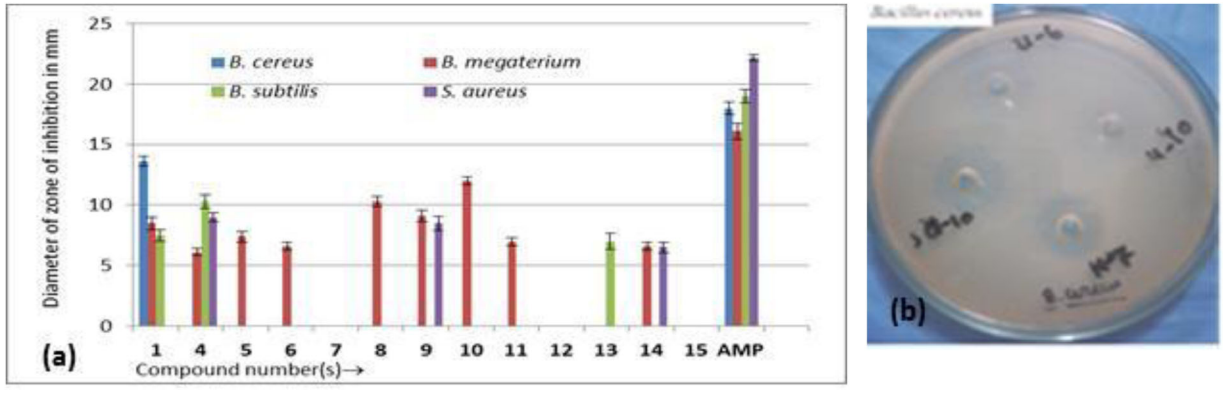

Figure 3. (a) Inhibition against Gram-positive bacteria; (b) Zone of inhibition observed against *Bacillus Cereus* by four test chemicals **13** (SO-10), **14** (K-7) and **15** (U-6).

both the Gram-positive and Gram-negative pathogens, and similar results were reported for other uridine esters (Kabir, Matin, & Kawsar, 1998; Kabir, Matin, Kawsar, & Anwar, 1998; Kabir, Matin, Mridha, et al., 1998; Kabir et al., 1998a, 1998b). Amongst the uridine derivatives, compound **8** (C6 chain) and **10** (C12 chain) showed moderate inhibition against *B. megaterium*, *S. dysenteriae* and *V. cholerae*. Also, mesyl derivative **6** and chlorobenzoyl derivatives **13**–**15** showed very little antibacterial functionality which is in agreement with the PASS results (Table 2). In general, compounds **4**–**15** were found more prone against Gram-negative pathogens than the Gram-positive organisms.

3.2.2. Antifungal susceptibility of 4–15

The susceptibility of uridine esters **4**–**15** against three pathogenic fungi are presented in Table 5. The results, as presented in percentage inhibitions of mycelial growth, indicated that these compounds were more prone against tested fungal pathogens compared to bacterial organisms. Among the tested fungi, **4**–**15** were more susceptible against *M. phaseolina*. Aliphatic chain containing compound **5** (C2, 57.8%, Figure 5), **8** (C6, 58.1%) and **10** (C12, 69.2%) exhibited very good percentage of inhibition against this fungus. To our surprise, chlorobenzoyl ester **14** (*72%) and **15** (*73.1%) showed excellent inhibition against *M. phaseolina* and the results were comparable to nystatin (*71.8%) in contrast to their antibacterial and PASS results.

3.3. Thermodynamic analysis

The molecular structure significantly influences the structural properties such as free energy (*G*), enthalpy (*H*), dipole moment and electrostatic potential. Spontaneity of a reaction and stability of a product can be predicted from Gibb's free energy, enthalpy and electronic energy. Free energy (*G*) is a significant criterion to represent the interaction of binding partners, where negative value favorable for spontaneous binding and interaction. Greater negative values predict better thermodynamic properties. In the present study, all the uridine esters possess greater negative value for *E*, *H* and *G* than the parent uridine, and hence, indicated that the attachment of ester group could improve interaction and binding of these molecules with different microbial enzymes. Due to these higher values (–2990 to –3903 Hartree) chlorobenzoyl esters **14**–**15** exhibited better inhibition against *M. phaseolina*. In addition, these increased negative values of compound **4–15** suggested that these are energetically and configurationally more stable.

Table 4. Inhibition against Gram-negative pathogens by **4**–**15**.

	Diameter of zone of inhibition in mm (100 μg dw/disc)				
Drug	*E. coli*	*S. dysenteriae*	*S. paratyphi*	*S. typhi*	*V. cholerae*
1	8.6 ± 0.50	NI	NI	10.5 ± 0.50	NI
4	7.5 ± 0.44	NI	8.0 ± 0.24	*12.5 ± 0.50	5.0 ± 0.44
5	NI	6.0 ± 0.58	NI	NI	NI
6	NI	8.4 ± 0.33	NI	NI	6.1 ± 0.33
7	NI	NI	NI	NI	6.6 ± 0.33
8	NI	*13.8 ± 0.38	*12.8 ± 0.83	NI	8.2 ± 0.54
9	9.5 ± 0.50	6.7 ± 0.71	7.8 ± 0.58	NI	NI
10	11.5 ± 0.50	7.0 ± 0.33	8.0 ± 0.33	NI	*12.5 ± 0.50
11	NI	9.8 ± 0.68	NI	NI	9.0 ± 0.50
12	7.7 ± 0.64	NI	NI	NI	NI
13	9.0 ± 0.71	10.1 ± 0.64	NI	NI	10.3 ± 0.71
14	NI	NI	NI	NI	7.0 ± 0.48
15	NI	NI	NI	NI	NI
**AMP	*10.9 ± 0.49	*22.1 ± 0.68	*18.0 ± 0.58	*20.2 ± 0.24	*31.9 ± 0.74

Data are presented as (Mean ± *SD*).
*Significantly inhibition values.
**Reference antibiotic ampicillin (AMP; 50 μg/disc).
dw: dry weight; NI: no inhibition; NI was observed for control DMF; Values are represented for the triplicate of all the experiments.

Table 5. Inhibition against fungal pathogens by **4**–**15**.

	% Inhibition of fungal mycelial growth (100 μg dw/mL PDA)		
Drug	*A. acheraccus*	*A. flavus*	*M. phaseolina*
1	NI	NI	25.3 ± 0.28
4	6.9 ± 0.24	NI	38.4 ± 0.38
5	18.7 ± 0.64	NI	*57.8 ± 0.64
6	17.5 ± 0.54	NI	NI
7	19.0 ± 0.24	NI	52.3 ± 0.64
8	NI	34.2 ± 0.64	*58.1 ± 0.50
9	10.7 ± 0.44	15.2 ± 0.84	NI
10	34.3 ± 0.48	25.8 ± 0.28	*69.2 ± 0.50
11	NI	28.0 ± 0.50	48.0 ± 0.84
12	14.0 ± 0.29	NI	41.0 ± 0.54
13	8.0 ± 0.24	NI	46.1 ± 0.83
14	9.1 ± 0.64	5.5 ± 0.33	*72.0 ± 0.68
15	NI	NI	*73.1 ± 0.84
**NYS	22.0 ± 0.25	26.1 ± 0.29	*71.8 ± 0.58

Data are presented as (Mean ± *SD*).
*Significant inhibition.
**Reference antibiotic nystatin NYS, 100 μg/mL PDA.
dw: dry weight; NI: no inhibition; NI was observed for control DMF; Values are represented for the triplicate of all the experiments.

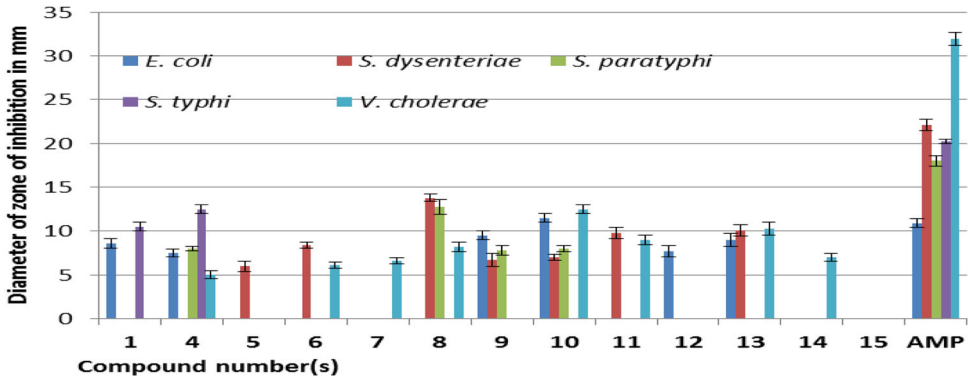

Figure 4. Inhibition against Gram-negative pathogens.

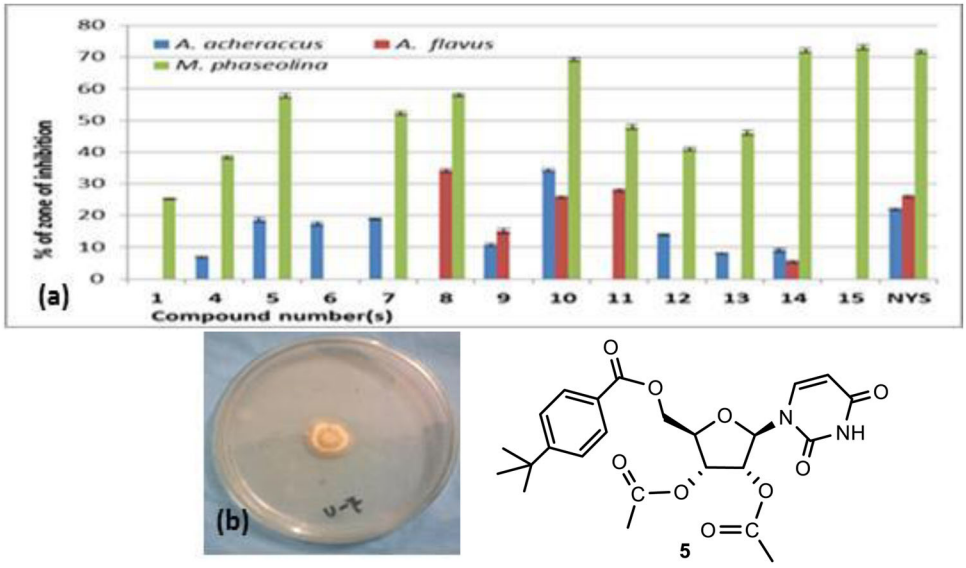

Figure 5. (a) Fungal inhibition by the uridine esters; (b) % Inhibition of mycelial growth of *A. acheraccus* by the **5** (U-7).

Table 6. Molecular formula, molecular weight, electronic energy (*E*), enthalpy (*H*), Gibb's free energy (*G*) in Hartree and dipole moment (μ, Debye) of uridine derivatives.

Drug	MF	MW	*E*	*H*	*G*	*μ*
1	$C_9H_{12}N_2O_6$	244.201	−900.579	−900.578	−900.635	7.339
4	$C_{20}H_{24}N_2O_7$	404.414	−1396.029	−1396.028	−1396.113	7.588
5	$C_{24}H_{28}N_2O_9$	488.487	−1697.825	−1697.824	−1697.924	3.865
6	$C_{22}H_{28}N_2O_{11}S_2$	560.595	−2562.166	−2562.165	−2562.270	5.001
7	$C_{30}H_{40}N_2O_9$	572.647	−1930.556	−1930.555	−1930.676	4.123
8	$C_{32}H_{44}N_2O_9$	600.700	−2008.131	−2008.130	−2008.257	4.166
9	$C_{40}H_{60}N_2O_9$	712.912	−2318.429	−2318.428	−2318.583	4.230
10	$C_{44}H_{68}N_2O_9$	769.019	−2473.580	−2473.579	−2473.746	2.274
11	$C_{48}H_{76}N_2O_9$	825.125	−2628.727	−2628.726	−2628.909	4.249
12	$C_{52}H_{84}N_2O_9$	881.231	−2783.876	−2783.875	−2784.072	4.253
13	$C_{34}H_{30}Cl_2N_2O_9$	681.516	−2990.069	−2990.068	−2990.189	6.206
14	$C_{34}H_{30}Cl_2N_2O_9$	681.516	−2990.070	−2990.069	−2990.190	6.300
15	$C_{34}H_{28}Cl_4N_2O_9$	750.406	−3903.457	−3903.456	−3903.584	7.619

As shown in Table 6, some of the uridine esters have improved dipole moment. Improved dipole moment enhances the polar nature of a molecule, and promotes the binding affinity, hydrogen bonding and nonbonding interaction with the receptor protein (Lien et al., 1982). The dipole moment of compound **4** was 7.588 Debye and for compound **15** was 7.619 Debye which were slightly higher than the uridine (7.339 Debye) resulting their better binding affinity and interactions with the amino acid residues of receptor protein.

3.3.1. Frontier molecular orbital analysis

The HOMO and LUMO energies, HOMO-LUMO gap (Δ?), hardness (*η*), softness (*S*) and chemical potential (μ) index of all compounds are presented in Table 7 (Figure 6). According to the frontier molecular orbital theory, energies of HOMO and LUMO play an important role in chemical reactivity. The HOMO-LUMO gap is also related to the chemical hardness, softness, chemical potential and electrophilic index of a molecule (Cohen & Benson, 1993; Lien et al., 1982). Large HOMO-LUMO gap is responsible for high kinetic stability and low chemical reactivity. On the other hand, small HOMO-LUMO gap is important for low chemical stability, because addition of electrons to a high-lying LUMO and/or removal of electrons from a low-lying HOMO is energetically favorable in any potential reaction. In these esters **4**–**15**, Δ? value was found lower than uridine (**1**), and thus, favorable for energetically favorable reaction. We noticed that, with the increase of the number of ester group(s) and chain length (**4**–**15**) hardness of these compounds gradually decreased while their softness gradually increased. All these properties may contribute to show higher chemical activity and polarizability in the drug related chemical and biochemical functionalities.

3.4. Molecular docking results

Estimation of the feasible binding geometries and interactions between drugs and active site of proteins (Matin, Bhattacharjee, et al., 2019; Matin, Bhuiyan, et al., 2019) is obtained from molecular docking (Ghosh et al., 2020). Molecular docking score of esters **4**–**15** along with standard antibiotic ampicillin (AMP) and hydroxychloroquine (HCQ) are shown in Table 8. We calculated docking score (binding affinity) of **13**–**14**, as these chlorobenzoyl compounds showed promising antifungal activities, with lanosterol 14α-demethylase (CYP51A1) and *A. flavus* (1R51) while all the uridine esters were considered for COVID-19 main protease (7BQY). In addition, other uridine esters **4**–**12** expressed, in

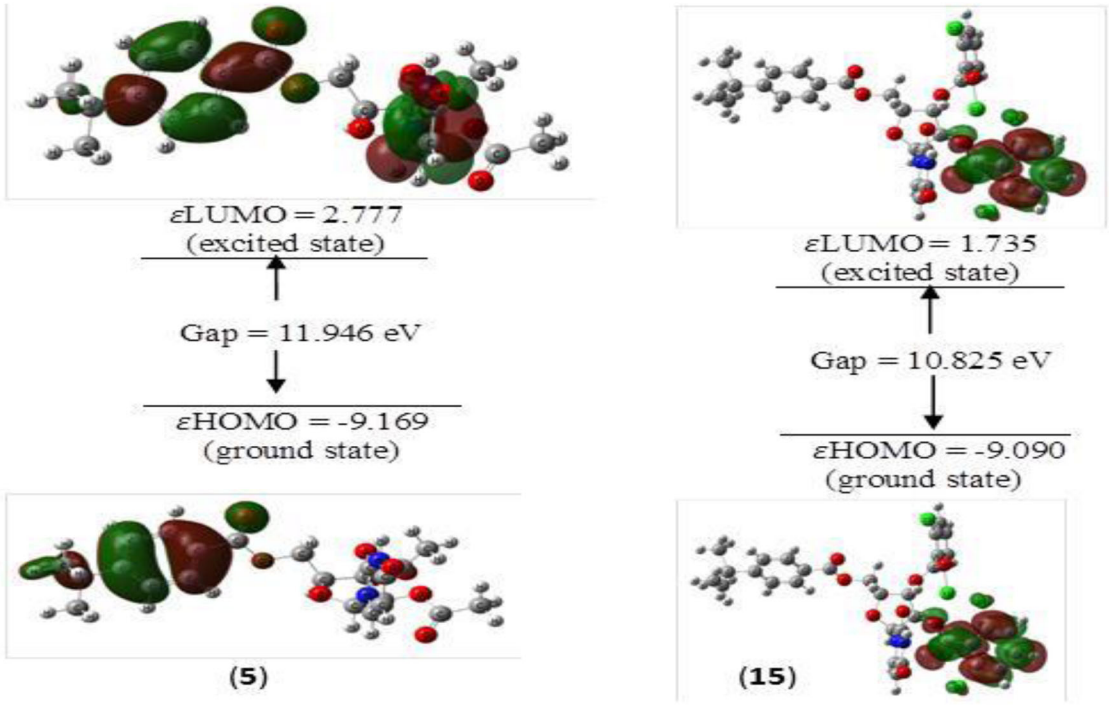

Figure **6.** Frontier molecular orbital and related energy of uridine derivatives **5** and **15**.

Table 7. Energy (eV) of HOMO, LUMO, Gap (Δ?), hardness (η), softness (S) and chemical potential (μ) of uridine (**1**) and its esters **4**–**15**.

Drug	HOMO	LUMO	Gap (Δ?)	η	S	μ
1	−9.896	2.848	12.744	6.372	0.157	−3.524
4	−9.157	2.812	11.969	5.985	0.167	−3.173
5	−9.169	2.777	11.946	5.973	0.167	−3.196
6	−9.262	2.638	11.900	5.950	0.168	−3.312
7	−9.154	2.798	11.952	5.976	0.167	−3.178
8	−9.152	2.801	11.953	5.977	0.167	−3.176
9	−9.149	2.804	11.953	5.977	0.167	−3.173
10	−9.144	2.811	11.955	5.978	0.167	−3.167
11	−9.148	2.805	11.953	5.977	0.167	−3.172
12	−9.148	2.805	11.953	5.977	0.167	−3.172
13	−9.174	1.771	10.945	5.473	0.183	−3.702
14	−9.239	1.781	11.020	5.510	0.181	−3.729
15	−9.090	1.735	10.825	5.413	0.185	−3.677

Table 8. Molecular docking score of **4**–**15**.

Drugs	CYP51A1 (kcal/mol)	1R51 (kcal/mol)	7BQY (kcal/mol)
4	−8.8	−8.1	−7.7
5	−9.0	−7.3	−7.9
6	−8.5	−7.2	−6.6
7	−7.5	−7.5	−8.0
8	−9.2	−6.4	−8.0
9	−9.0	−6.0	−6.4
10	−5.4	−5.8	−5.5
11	−6.6	−6.3	−4.9
12	−4.5	−5.8	−5.2
13	−12.0	−9.3	−7.7
14	−11.1	−7.7	−7.6
15	−8.3	−8.0	−7.8
AMP	−7.9	−7.5	–
HCQ	–	–	−6.1

average, somewhat lower docking score than **13**–**14** against CYP51A1 and 1R51.

Ampicillin (AMP) and HCQ were used as standard drugs; Discovery Studio (version 4.1) was performed for analysis and view of docking results.

Docking score clearly indicated that chlorobenzoyl esters **13**–**15** had binding energy with both the CYP51A1 (−7.9 to −12.0 kcal/mol; Figure 7(a,b)) and 1R51 (−7.5 to −9.3 kcal/mol; Figure 7(c,d)) proteins which were higher than the standard antibiotic ampicillin (−7.9 and −7.5 kcal/mol). The results are in complete accord with the *in vitro* results (Table 5) that these uridine esters had better antifungal activities.

Considering the current COVID-19 pandemic caused by the SARS-CoV-2 betacoronavirus (Ghosh et al., 2020; Lakshmi et al., 2020) we have extended our studies by docking with COVID-19 main protease (7BQY). As shown in Table 8, most of the uridine esters showed higher binding affinity with 7BQY than HCQ (−6.1 Kcal/mol). It is worth to mention that saturated fatty acyl esters with **5**, **7**–**8** smaller chain length exhibited better binding affinity than the higher chain length **9**–**12**, sulphonyl ester **6** and chlorobenzoyl esters **13**–**15** (Figure 8). The docking score of **5**, **7** and **8** (−7.9 to −8.0 kcal/mol) were found to better than the previously published other compounds (Ghosh et al., 2020). Thus, uridine aliphatic esters could be better choice than HCQ in treating COVID-19 infection.

3.5. Cytotoxic activity of the uridine esters 4–15

The toxicity activity of the acylated uridine derivatives **4**–**15** in the brine shrimp lethality bioassay method (McLaughlin, 1991) is presented in Figure 9, which showed the percentage of mortality of shrimps at 24 h and 48 h. From the data, it was evident that the test chemicals 5′-*O*-(4-*t*-butylbenzoyl)-2′,3′- di- *O*- pentanoyl-uridine (**7**) and 5′-*O*-(4-*t*-butylbenzoyl)-2′,3′-di-*O*-lauroyluridine (**10**) showed highest levels of toxicity (i.e. ∼57% death) indicating its higher mortality. The rest of the compounds were found less toxic for brine shrimp (Figure 9).

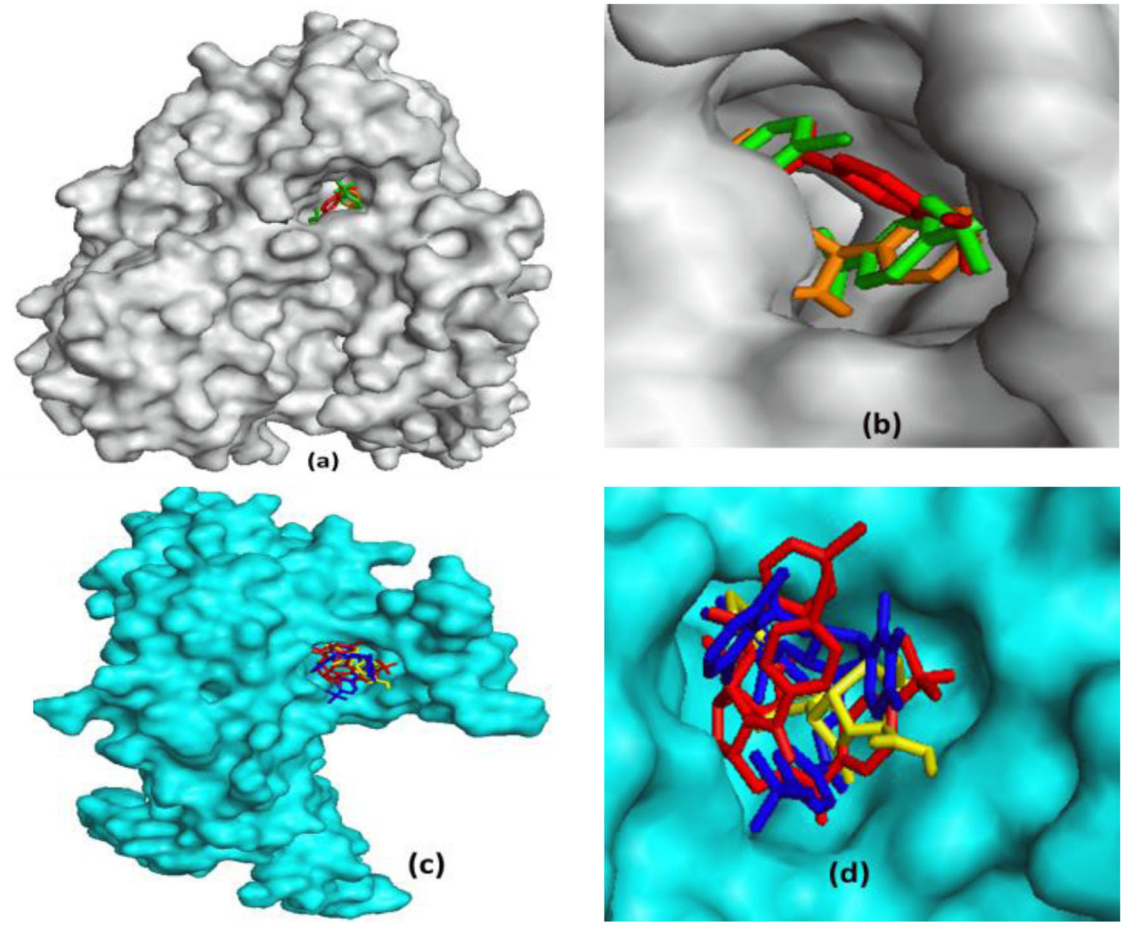

Figure 7. (a) Docking pose (represented in space-filling model) of **13**, **14** and ampicillin with CYP51A1; (b) 2D interaction map of **13**, **14** and ampicillin with CYP51A1; (c) Docking pose of **14**, **15** and ampicillin with 1R51; (d) 2D interaction map of **14**, **15** and ampicillin with 1R51.

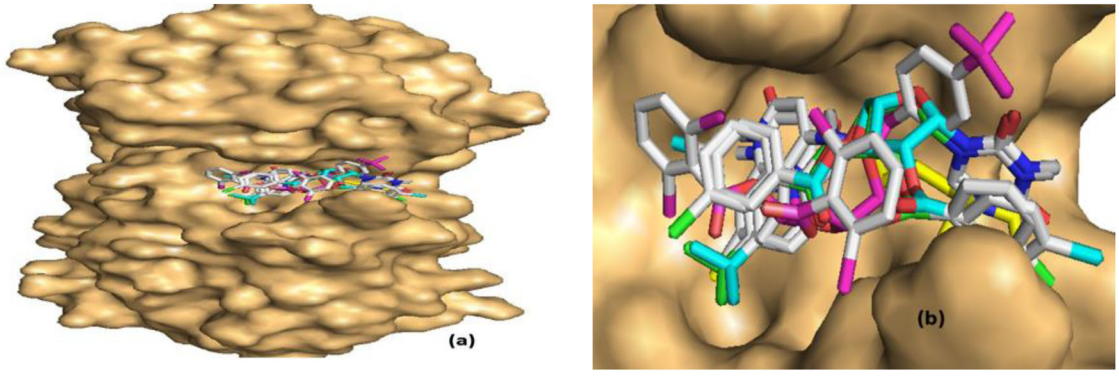

Figure 8. (a) Docked pose (represented in space-filling model) and (b) 2D interaction map of **13**, **14, 15** and HCQ with 7BQY.

3.6. ADME/T properties

Absorption, distribution, metabolism, excretion and toxicity (ADMET) related pharmacokinetic profile is mentioned in Table 9. It is evident that these compounds possess better absorption value than standard antibiotics (ampicillin and nystatin) although they are P-glycoprotein inhibitor (except **15**). Distribution like BBB (>−1) and CNS (>−2) permeability values are comparable to standard drugs. Compounds **4**–**14** are CYP3A4 enzyme substrate while **15** is non-substrate for this enzyme. Their excretion, presented as total clearance, is comparable to ampicillin.

We have also calculated their toxicity values along with standard antibiotics. hERG (human ether-à-go-go-related gene I) showed negative values for these compounds like nystatin. Hence, these compounds could be safe and will not generate QT syndrome like fatal ventricular arrhythmia (Matin, Bhattacharjee, et al., 2019; Matin, Bhuiyan, et al., 2019; Matin, Chakraborty, et al., 2020). In addition, it is important to consider the lethal dosage (LD_{50}) values and is

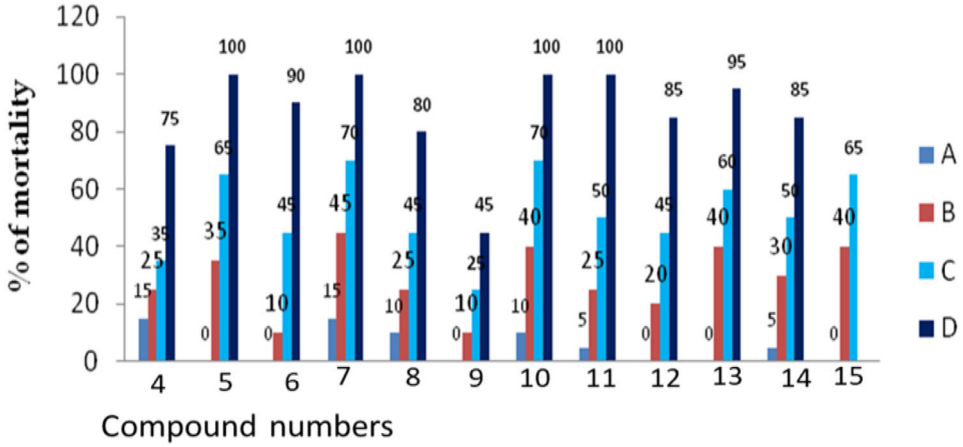

Figure 9. Cytotoxic activity of the uridine esters **4**–**15**.

Table 9. ADMET calculation of uridine derived esters **4**–**15**.

	Absorption			Distribution		Metabolism	Excretion	Toxicity	
Drug	C2P	HIA (%)	P-gpl	BBB (permeability)	CNS	CYP3A4 substrate	Total clearance	hERG inhibitor	Acute LD50
1	−0.149	50.745	No	−1.401	−4.44	No	0.662	No	2.032
4	0.849	64.746	Yes	−1.269	−3.577	Yes	1.05	No	2.156
5	−0.307	73.091	Yes	−1.516	−3.533	Yes	0.675	No	1.94
6	−0.356	64.449	Yes	−2.322	−4.004	Yes	0.519	No	2.068
7	−0.386	80.936	Yes	−1.038	−3.206	Yes	0.79	No	2.379
8	−0.431	76.614	Yes	−1.042	−3.11	Yes	0.822	No	2.588
9	−0.654	82.458	Yes	−1.081	−2.883	Yes	0.943	No	2.866
10	−0.764	85.355	Yes	−1.099	−2.836	Yes	0.855	No	2.769
11	−0.874	88.256	Yes	−1.117	−2.79	Yes	0.913	No	2.645
12	−0.984	91.157	Yes	−1.136	−2.743	Yes	0.972	No	2.543
13	−0.311	97.276	Yes	−1.155	−2.956	Yes	0.377	No	2.317
14	−0.213	97.221	Yes	−1.188	−2.936	Yes	0.503	No	2.315
15	−0.276	100	No	−1.554	−2.846	No	0.026	No	2.284
AMP	0.395	43.034	No	−0.767	−3.166	No	0.337	No	1.637
NYS	−0.609	0.00	No	−2.09	−3.702	No	−1.357	No	2.518

C2P: Caco-2 permeability (log Papp in 10^{-6} cm/s, >0.90 indicates high permeability); HIA: Human intestinal absorption (% absorbed, >30% is better absorbed); P-gpI: P-glycoprotein inhibitor; BBB (blood brain barrier) is expressed in logBB (logBB >-1.0 is moderately cross blood brain barrier); CNS (central nervous system) is expressed as logPS (logPS > −2.0 can easily penetrate the CNS); Total clearance is expressed in log mL/min/kg; hERG: human ether-à-go-go-related gene I; Toxicity is calculated in oral rat acute toxicity (mol/kg); AMP: ampicillin; NYS: nystatin.

Table 10. Calculation drug likeness using SwissADME.

Drug	HB acceptors	HB donors	TPSA Å^2	CYP1A2 inhibitor	CYP2C19 inhibitor	CYP2C9 inhibitor	CYP2D6 inhibitor	CYP3A4 inhibitor	PAINS alerts
1	6	4	124.78	No	No	No	No	No	0
4	7	3	130.85	No	No	No	No	No	0
5	9	1	142.99	No	No	No	No	Yes	0
6	11	1	193.89	No	No	No	No	Yes	0
7	9	1	142.99	No	No	Yes	Yes	Yes	0
8	9	1	142.99	No	No	Yes	Yes	Yes	0
9	9	1	142.99	No	No	No	No	No	0
10	9	1	142.99	No	No	No	No	No	0
11	9	1	142.99	No	No	No	No	No	0
12	9	1	142.99	No	No	No	No	No	0
13	9	1	142.99	No	No	Yes	No	No	0
14	9	1	142.99	No	No	Yes	No	No	0
15	9	1	142.99	No	No	No	No	No	0
AMP	5	3	138.03	No	No	No	No	No	0
NYS	18	12	319.61	No	No	No	No	No	0

*HB: hydrogen bond; TPSA: topological polar surface area, PAINS: Pan-assay interference compounds, AMP: ampicillin, NYS: nystatin.

used to assess the relative toxicity of different molecules. Here, most of the ester's LD_{50} values (<3 mol/kg) are in good consistent with the value of nystatin (2.52 mol/kg).

Drug likeness calculations were calculated from SwissADME tool and are summarized in Table 10. For comparison both the uridine esters and standard antibiotics'

drug likeness values were calculated. It was found that all the esters (except mesylate **6**) have good hydrogen bonds donor and acceptor which is in consistent with the Lipnski's rule of five. The more the value topological polar surface area (TPSA) more the polarity of the compounds and should be less than 140 Å^2. The TPSA in these molecules was in excellent agreement (∼143 Å^2) with the most important rules of drug likeness (Lipinski et al., 1997).

In the present study, we have checked the CYP enzymes, particularly isoforms 1A2, 2C9, 2C19, 2D6 and 3A4, inhibitory activities which are responsible for about 90% oxidative metabolic reactions. Inhibition of CYP enzymes will lead to inductive or inhibitory failure of drug metabolism. These inhibitions of compound **4**, **9**–**12** and **15** were found similar to that of the standard drugs (Table 10). In addition, Pan-assay interference compounds (PAINS) revealed no violation with these uridine esters. PAINS are chemical compounds that often give false positive results in high-throughput screens. PAINS tend to react nonspecifically with numerous biological targets rather than specifically affecting one desired target. Many studies indicated the acute toxic effects of medicines on non-targeted organisms, and hence, the MTT, MTS and Resazurin assay methods are used to check the cytotoxic concentration of any new molecule (synthetic or natural) which gives an idea about the maximum nontoxic dose of the drug molecule. We hope to conduct such studies for the more drug related validation of these promising uridine compounds.

3.7. Structure–activity relationship

It was observed that the most of the potential antifungal drugs (fluconazole; itraconazole; voriconazole; terbinafine) are designed to deter the activity of CYP51A1 enzyme to synthesize essential ergosterol (Matin, Chakraborty, et al., 2020; Matin, Hasan, et al., 2020; Matin, Roshid, et al., 2020). On the basis of our study, it could be thought that the effective uridine esters **13**–**15** restricted CYP51 enzyme activity by binding with it, and hence, fungal ergosterol could not form. The unavailability of ergosterol ultimately causes disruption of the fungal cell wall causing organisms death.

On the other hand, saturated fatty acyl esters with **5**, **7**–**8** smaller chain length (C2–C6) showed slightly better binding score (–7.9 to –8.0 kcal/mol) than chlorobenzoyl esters **13**–**15** (–7.6 to –7.8 kcal/mol) with 7BQY (COVID-19 main protease). Methanesuphonyl ester **6** (–6.6 kcal/mol) and HQC (–6.1 kcal/mol) had lower binding energy. The present results, thus, might have pave the way for discovery of novel drugs related to COVID-19 treatment although related further study is needed.

4. Conclusion

Covid-19, toxicity and evolution of MDR organisms in the microbial world caused a huge threat, and hence, novel antiviral and antimicrobial drugs preferably with newer mode of action, and reduced side-effects are essential. In this context several uridine esters were analyzed *in vitro* and *in silico* for their antimicrobial, thermodynamic, molecular docking and drug likeness properties. The study revealed that chloro-substituted benzoyl esters **13**–**15** of uridine were more potential against fungal organisms with better pharmacokinetic and drug likeness spectra. In addition, some aliphatic acyl esters especially with lower carbon chains (C2-C6) showed promising binding score with COVID-19 main protease (7BQY). In this promising context, more drug likeness *in vitro* and *in vivo* study such as nontoxic concentration towards healthy cells may be conducted in the near future.

Acknowledgements

S. A. Chowdhury would like to thank Ministry of Science and Technology, Bangladesh for PhD fellowship. The authors are grateful to the Institute of Marine Science, University of Chittagong, Bangladesh and the Department of Physiology, Biochemistry & Pharmacology, University of Chittagong Veterinary and Animal Science, Bangladesh for providing facilities during cytotoxic and antimicrobial evaluation.

Disclosure statement

No potential conflict of interest was reported by the authors.

Funding

M. M. Matin acknowledges Research Cell, University of Chittagong, Bangladesh (2019-20) for providing partial financial support. Also, the financial contribution (grant no. PS 201660, 2016-17) from the Ministry of Education, Bangladesh and BANBEIS is appreciated.

ORCID

Mohammed Mahbubul Matin https://orcid.org/0000-0003-4965-2280
Monir Uzzaman https://orcid.org/0000-0002-6887-9344

References

Awual, M. R. (2017). New type mesoporous conjugate material for selective optical copper(II) ions monitoring & removal from polluted waters. *Chemical Engineering Journal*, *307*, 85–94. https://doi.org/10.1016/j.cej.2016.07.110

Banasch, M., Goetze, O., Knyhala, K., Potthoff, A., Schlottmann, R., Kwiatek, M. A., Bulut, K., Schmitz, F., Schmidt, W. E., & Brockmeyer, N. H. (2006). Uridine supplementation enhances hepatic mitochondrial function in thymidine-analogue treated HIV-infected patients. *AIDS (London, England)*, *20*(11), 1554–1556. https://doi.org/10.1097/01.aids.0000237373.38939.14

Carlezon, W. A., Jr., Mague, S. D., Parow, A. M., Stoll, A. L., Cohen, B. M., & Renshaw, P. F. (2005). Antidepressant-like effects of uridine and omega-3 fatty acids are potentiated by combined treatment in rats. *Biological Psychiatry*, *57*(4), 343–350. https://doi.org/10.1016/j.biopsych.2004.11.038

Chowdhury, S. A., Bhuiyan, M. M. R., Ozeki, Y., & Kawsar, S. M. A. (2016). Simple and rapid synthesis of some nucleoside derivatives: Structural and spectral characterization. *Current Chemistry Letters*, *5*(2), 83–92. https://doi.org/10.5267/j.ccl.2015.12.001

Clayden, J., Greeves, N., Warren, S., & Wothers, P. (2012). *Organic chemistry* (2nd ed., p. 1234). Oxford University Press.

Cohen, N., & Benson, S. W. (1993). Estimation of heats of formation of organic compounds by additivity methods. *Chemical Reviews*, *93*(7), 2419–2438. https://doi.org/10.1021/cr00023a005

De Clercq, E. (2011). A 40-year journey in search of selective antiviral chemotherapy. *Annual Review of Pharmacology and Toxicology*, *51*, 1–24. https://doi.org/10.1146/annurev-pharmtox-010510-100228

Dobolyi, A., Juhász, G., Kovács, Z., & Kardos, J. (2011). Uridine function in the central nervous system. *Current Topics in Medicinal Chemistry*, *11*(8), 1058–1067. https://doi.org/10.2174/156802611795347618

Du, L.-H., Shen, J.-H., Dong, Z., Zhou, N.-N., Cheng, B.-Z., Ou, Z.-M., & Luo, X.-P. (2018). Enzymatic synthesis of nucleoside analogues from uridines and vinyl esters in a continuous-flow microreactor. *RSC Advances*, *8*(23), 12614–12618. https://doi.org/10.1039/c8ra01030g

Escober, J. F. B., Carmona, V. H. A., Jaramillo, E. G., Margarita, D. M. M., Fernández, M. E. M., Guerrero, M. C., & Martínez, A. M. (2016). Synthesis and cytotoxic activity of tri-acyl ester derivatives of uridine in breast cancer cells. *Ars Pharmaceutica*, *57*(4), 183–191. https://doi.org/10.4321/S2340-98942016000400005

Ghosh, R., Chakraborty, A., Biswas, A., & Chowdhuri, S. (2020). Evaluation of green tea polyphenols as novel corona virus (SARS CoV-2) main protease (Mpro) inhibitors – an *in silico* docking and molecular dynamics simulation study. *Journal of Biomolecular Structure and Dynamics*. https://doi.org/10.1080/07391102.2020.1779818

Kabir, A. K. M. S., Matin, M. M., Ali, M., & Anwar, M. N. (2003). Comparative studies on selective acylation and antimicrobial activities of some D-glucofuranose derivatives. *Journal of Bangladesh Academy of Sciences*, *27*(1), 43–50.

Kabir, A. K. M. S., Matin, M. M., Islam, K. R., & Anwar, M. N. (2002). Synthesis and antimicrobial activities of some acylated uridine derivatives. *Journal of the Bangladesh Chemical Society*, *15*(1), 13–22.

Kabir, A. K. M. S., Matin, M. M., & Kawsar, S. M. A. (1997). Selective acylation of uridine using the dibutyltin oxide and direct methods. *Chittagong University Studies, Part II: Science*, *21*(2), 39–45.

Kabir, A. K. M. S., Matin, M. M., & Kawsar, S. M. A. (1998). Synthesis and antibacterial activities of some uridine derivatives. *The Chittagong University Journal of Science*, *22*(1), 13–18.

Kabir, A. K. M. S., Matin, M. M., Kawsar, S. M. A., & Anwar, M. N. (1998). Antibacterial activities of some selectively acylated uridine derivatives. *The Chittagong University Journal of Science*, *22*(2), 37–41.

Kabir, A. K. M. S., Matin, M. M., Mridha, M. A. U., & Shahed, S. M. (1998). Antifungal activities of some methyl 6-*O*-trityl-α-D-mannopyranosides. *The Chittagong University Journal of Science*, *22*(1), 41–46.

Kabir, A. K. M. S., Matin, M. M., & Uddin, M. R. (1998a). Comparative studies on selective acylation of uridine using the dibutyltin oxide and direct methods. *The Chittagong University Journal of Science*, *22*(1), 97–103.

Kabir, A. K. M. S., Matin, M. M., & Uddin, M. R. (1998b). Selective myristoylation and palmitoylation of uridine. *The Chittagong University Journal of Science*, *22*(2), 27–35.

Kruse, H., Goerigk, L., & Grimme, S. (2012). Why the standard B3LYP/6-31G* model chemistry should not be used in DFT calculations of molecular thermochemistry: Understanding and correcting the problem. *The Journal of Organic Chemistry*, *77*(23), 10824–10834. https://doi.org/10.1021/jo302156p

Lakshmi, S. A., Shafreen, R. M. B., Priya, A., & Shunmugiah, K. P. (2020). Ethnomedicines of Indian origin for combating COVID-19 infection by hampering the viral replication: Using structure-based drug discovery approach. *Journal of Biomolecular Structure and Dynamics*. https://doi.org/10.1080/07391102.2020.1778537

Laws, M., Surani, Y. M., Hasan, M. M., Chen, Y., Jin, P., Al-Adhami, T., Chowdhury, M., Imran, A., Psaltis, I., Jamshidi, S., Nahar, K. S., & Rahman, K. M. (2020). Current trends and future approaches in small-molecule therapeutics for COVID-19. *Current Medicinal Chemistry*, *27*. https://doi.org/10.2174/0929867327666200721161840

Lien, E. J., Guo, Z.-R., Li, R.-L., & Su, C.-T. (1982). Use of dipole moment as a parameter in drug-receptor interaction and quantitative structure-activity relationship studies. *Journal of Pharmaceutical Sciences*, *71*(6), 641–655. https://doi.org/10.1002/jps.2600710611

Lipinski, C. A., Lombardo, F., Dominy, B. W., & Feeney, P. J. (1997). Experimental and computational approaches to estimate solubility and permeability in drug discovery and development settings. *Advanced Drug Delivery Reviews*, *23*(1–3), 3–25. https://doi.org/10.1016/S0169-409X(96)00423-1

Lucido, M. J., Orlando, B. J., Vecchio, A. J., & Malkowski, M. G. (2016). Crystal structure of aspirin-acetylated human cyclooxygenase-2: Insight into the formation of products with reversed stereochemistry. *Biochemistry*, *55*(8), 1226–1238. https://doi.org/10.1021/acs.biochem.5b01378

Matin, M. M. (2008). Synthesis of D-glucose derived oxetane: 1,2-*O*-isopropylidene-4-(*S*)-3-*O*,4-*C*-methylene-5-*O*-methanesulfonyl-β-L-threo-pento-1,4-furanose. *Journal of Applied Sciences Research*, *4*(11), 1478–1482.

Matin, M. M. (2014). Synthesis and antimicrobial study of some methyl 4-*O*-palmitoyl-α-L-rhamnopyranoside derivatives. *Orbital: The Electronic Journal of Chemistry*, *6*(1), 20–28. https://doi.org/10.17807/orbital.v6i1.553

Matin, M. M., Bhattacharjee, S. C., Chakraborty, P., & Alam, M. S. (2019). Synthesis, PASS predication, in vitro antimicrobial evaluation and pharmacokinetic study of novel *n*-octyl glucopyranoside esters. *Carbohydrate Research*, *485*, 107812. https://doi.org/10.1016/j.carres.2019.107812

Matin, M. M., Bhuiyan, M. M. H., Azad, A. K. M. S., & Akther, N. (2017). Design and synthesis of benzyl 4-*O*-lauroyl-α-L-rhamnopyranoside derivatives as antimicrobial agents. *Current Chemistry Letters*, *6*(1), 31–40. https://doi.org/10.5267/j.ccl.2016.10.001

Matin, M. M., Bhuiyan, M. M. H., Debnath, D. C., & Manchur, M. A. (2013). Synthesis and comparative antimicrobial studies of some acylated D-glucofuranose and D-glucopyranose derivatives. *International Journal of Biosciences*, *3*(8), 279–287. https://doi.org/10.12692/ijb/3.8.279-287

Matin, M. M., Bhuiyan, M. M. H., Hossain, M. M., & Roshid, M. H. O. (2015). Synthesis and comparative antibacterial studies of some benzylidene monosaccharide benzoates. *Journal of the Turkish Chemical Society, Section A: Chemistry*, *2*(4), 12–21. https://doi.org/10.18596/jotcsa.83708

Matin, M. M., Bhuiyan, M. M. H., Kabir, E., Sanaullah, A. F. M., Rahman, M. A., Hossain, M. E., & Uzzaman, M. (2019). Synthesis, characterization, ADMET, PASS predication, and antimicrobial study of 6-*O*-lauroyl mannopyranosides. *Journal of Molecular Structure*, *1195*, 189–197. https://doi.org/10.1016/j.molstruc.2019.05.102

Matin, M. M., Chakraborty, P., Alam, M. S., Islam, M. M., & Hanee, U. (2020). Novel mannopyranoside esters as sterol 14α-demethylase inhibitors: Synthesis, PASS predication, molecular docking, and pharmacokinetic studies. *Carbohydrate Research*, *496*, 108130. https://doi.org/10.1016/j.carres.2020.108130

Matin, M. M., Hasan, M. S., Uzzaman, M., Bhuiyan, M. M. H., Kibria, S. M., Hossain, M. E., & Roshid, M. H. O. (2020). Synthesis, spectroscopic characterization, molecular docking, and ADMET studies of mannopyranoside esters as antimicrobial agents. *Journal of Molecular Structure*, *1222*, 128821. https://doi.org/10.1016/j.molstruc.2020.128821

Matin, M. M., & Ibrahim, M. (2010). Synthesis of some methyl 4-*O*-octnoyl-α-L-rhamnopyranoside derivatives. *Journal of Applied Sciences Research*, *6*(10), 1527–1532.

Matin, M. M., Nath, A. R., Saad, O., Bhuiyan, M. M. H., Kadir, F. A. A., Hamid, S. B. A., Alhadi, A. A., Ali, M. E., & Yehye, W. A. (2016). Synthesis, PASS-predication and in vitro antimicrobial activity of benzyl 4-*O*-benzoyl-α-L-rhamnopyranoside derivatives. *International Journal of Molecular Sciences*, *17*(9), 1412. https://doi.org/10.3390/ijms17091412

Matin, M. M., Roshid, M. H. O., Bhattacharjee, S. C., & Azad, A. K. M. S. (2020). PASS Predication, antiviral, *in vitro* antimicrobial, and ADMET studies of rhamnopyranoside esters. *Medical Research Archives*, *8*(7), 2165. https://doi.org/10.18103/mra.v8i7.2165

McLaughlin, J. L. (1991). Crown-gall tumours in potato discs and brine shrimp lethality: Two simple bioassays for higher plant screening and fractionation. In K. Hostettmann (Ed.), *Methods in plant biochemistry: Assays for bioactivity* (Vol. 6, pp. 1-32). Academic Press.

Pearson, R. G. (1986). Absolute electronegativity and hardness correlated with molecular orbital theory. *Proceedings of the National Academy of Sciences of the United States of America*, *83*(22), 8440–8441. https://doi.org/10.1073/pnas.83.22.8440

Pires, D. E. V., Blundell, T. L., & Ascher, D. B. (2015). pkCSM: Predicting small-molecule pharmacokinetic and toxicity properties using graph-

based signatures. *Journal of Medicinal Chemistry*, *58*(9), 4066–4072. https://doi.org/10.1021/acs.jmedchem.5b00104

Sharavanan, V. J., Sivaramakrishnan, M., Sivarajasekar, N., Senthilrani, N., Kothandan, R., Dhakal, N., Sivamani, S., Show, P. L., Awual, M. R., & Naushad, M. (2020). Pollutants inducing epigenetic changes and diseases. *Environmental Chemistry Letters*, *18*(2), 325–343. https://doi.org/10.1007/s10311-019-00944-3

Siegel, D., Hui, H. C., Doerffler, E., Clarke, M. O., Chun, K., Zhang, L., Neville, S., Carra, E., Lew, W., Ross, B., Wang, Q., Wolfe, L., Jordan, R., Soloveva, V., Knox, J., Perry, J., Perron, M., Stray, K. M., Barauskas, O., … Mackman, R. L. (2017). Discovery and synthesis of a phosphoramidate prodrug of a Pyrrolo[2,1-f][triazin-4-amino] adenine C-nucleoside (GS-5734) for the treatment of ebola and emerging viruses. *Journal of Medicinal Chemistry*, *60*(5), 1648–1661. https://doi.org/10.1021/acs.jmedchem.6b01594

Strasser, S., Maier, S., Leisser, C., Saiko, P., Madlener, S., Bader, Y., Bernhaus, A., Gueorguieva, M., Richter, S., Mader, R. M., Wesierska-Gadek, J., Schott, H., Szekeres, T., Fritzer-Szekeres, M., & Krupitza, G. (2006). 5-FdUrd-araC heterodinucleoside re-establishes sensitivity in 5-FdUrd- and AraC-resistant MCF-7 breast cancer cells overexpressing ErbB2. *Differentiation; Research in Biological Diversity*, *74*(9–10), 488–498. https://doi.org/10.1111/j.1432-0436.2006.00082.x

Susilo, R. (Köln, DE). (2008). Pharmaceutically active uridine esters, United States, Trommsdorff GmbH & Co. KG Arzeneimittel (Alsdorf, DE) 7417034. http://www.freepatentsonline.com/7417034.html

Wahedi, H. M., Ahmad, S., & Abbasi, S. W. (2020). Stilbene-based natural compounds as promising drug candidates against COVID-19. *Journal of Biomolecular Structure and Dynamics*. https://doi.org/10.1080/07391102.2020.1762743

Yamamoto, T., Koyama, H., Kurajoh, M., Shoji, T., Tsutsumi, Z., & Moriwaki, Y. (2011). Biochemistry of uridine in plasma. *Clinica Chimica Acta; International Journal of Clinical Chemistry*, *412*(19–20), 1712–1724. https://doi.org/10.1016/j.cca.2011.06.006